Available online at www.sciencedirect.com

ScienceDirect

Procedia Engineering 6 (2010) 133–142

Procedia Engineering

www.elsevier.com/locate/procedia

IUTAM Symposium on Computational Aero-Acoustics
for Aircraft Noise Prediction

Time Domain Impedance Modelling and Applications

Christoph Richter[a], Junis Abdel-Hay[b], Łukasz Panek[b], Norbert Schönwald[b], Stefan Busse[b], Frank Thiele[b]

[a]*Technische Universität Berlin, Institute of Fluid Mechanics and Engineering Acoustics, christoph.richter@tu-berlin.de*
[b]*Technische Universität Berlin, Institute of Fluid Mechanics and Engineering Acoustics*

Abstract

Today, there is a high, often not fully evolved potential of noise attenuation by passive acoustic treatments. Current numerical methods are able to help developing optimal treatments. Thus, the simulation of acoustic lining in aeroengines is one of the core objectives for the development of modern CAA solvers. Here, the opportunities of the Extended Helmholtz Resonator (EHR) model of Rienstra in the time domain in this design and optimisation process are demonstrated. The optimization of a lining for a specific application as the obvious objective is still out of reach for many cases with current numerical resources. However, the model allows the optimisation towards the dissipation characteristics in an impedance flow tube measurement with a physical liner sample, which provides the numerical parameters of the liner for high fidelity CAA simulations. Moreover, the model parameters are related to the cell geometry and face sheet of the liner panel. An example is provided for the purely numerical prediction of the attenuation in the complex flow of an aeroengine duct. This is demonstrated by considering the resulting parameters in modal axisymmetric and three dimensional simulations of the rearward sound radiation from a lined bypass duct. The example demonstrates, that the optimisation of the liner properties is not achievable in a justifiable time, even if simplified two dimensional conditions are considered. A possible solution to this problem is to use the computational power of a graphics processing unit (GPU). The development of pixel shaders which implement a large number of parallel processors into the GPU, shows a much more agile growth than any CPU based system does. As an outlook, a platform independent implementation of a GPU based CAA solver with impedance boundary condition and the capability to handle axisymmetric duct geometries is presented. It demonstrates a speed up by a factor > 100.

Keywords: time domain impedance modelling, CAA, GPU

1. Introduction

Aeroacoustic propagation codes for the simulation and optimisation of acoustic lining for aeroengine ducts require to account for arbitrary base flow conditions and transient and non-linear propagation phenomena. Thus, time-domain simulation methods and the related impedance boundary conditions are required for this purpose. These time-domain impedance boundary conditions usually consist of two parts. One is a physical model of the lining, describing the frequency response of the impedance surface and providing its time domain equivalent. A number of such models is addressed in section 2.1. The second is a method to account for the grazing flow conditions on the surface. The most simple method to account for grazing flow conditions would be a fully resolved boundary layer. However, this method would be the most demanding in terms of computational resources at the same time. The alternative is the Ingard/Myers boundary condition, which allows a larger mesh spacing and in consequence larger time steps, on the cost of being ill posed with flow. This flow model and the related problems are addressed in section 2.2. Different types

1877-7058
doi:10.1016/j.proeng.2010.09.015

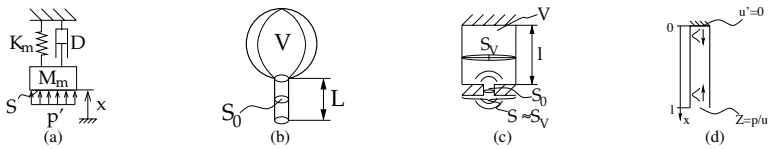

Figure 1: Representations of a locally reacting wall: (a) Mechanical analogue; (b) Helmholtz resonator; (c) Panel; (d) $\lambda/4$–resonator

of physical models for the lining are discussed and parallels of different models are shown. These parallels provide links between the model parameters in the low frequency range. This shows the possibility to identify the model parameters with the typical dimensions of the liner. The implementation of the Extended Helmholtz Resonator model of Rienstra [1], with a finite difference based CAA method based on the DRP and LDDRK schemes is discussed in detail in section 2.3. The model parameters of the time domain impedance boundary condition are determined from experimental energy reflection and transmission measurements in an impedance flow tube via optimisation in section 3. The result is reviewed using the experimental data and the measurable dimensions of the liner in comparison to the numerical result and the resulting geometry in section 3.2. The educed model parameters of a liner sample are then applied in a three dimensional simulation. The effect of this liner on the sound propagation in a bypass duct of a long-cowl aeroengine is studied under take-off conditions. Altogether, the processing chain for a high fidelity CAA simulation with liner in ducted environments is established. Starting from the experiment with a liner sample under grazing flow conditions, the model parameters of the impedance boundary condition are determined via optimisation and then applied in modal axisymmetric and three dimensional simulations of the sound propagation in a realistic geometry under realistic flow conditions. The potential of running a time domain CAA method with impedance boundary condition using the high performance of a modern graphics processor is finally presented in section 8.

2. Time domain impedance modelling

At first in this section, an overview on some physical impedance models in the frequency domain is presented. One of them is the extended Helmholtz resonator model by Rienstra [1]. The implementation of this extended Helmholtz resonator model to a time domain CAA method is discussed at the end of the section. Before that, the treatment of a non-zero base flow on the surface is discussed.

2.1. A recapitulation of some impedance models in the frequency domain

2.1.1. Low frequency mechanical analogue for the resonator (Figure 1(a))

The mass-spring-damper element shown in Figure 1(a) is forced by the acoustic pressure on the surface of the mass. The equation of motion reads $M_m\,\ddot{x} = S\,p' - K_m\,x - D\,\dot{x}$. The mechanical model parameters are related to the cavity volume V, the neck length L and the open area of the neck S_0 shown in Figure 1(b). The equation of motion is rewritten and the mechanical analogue is used to identify the moving mass with the air in the neck and the spring with the compressed air in the cavity, yielding

$$Z_{\mathrm{HR}} = i\omega\varrho_0\,L + d + i\omega^{-1}\,S_0\,\varrho_0\,c^2V^{-1}. \tag{1}$$

The mechanical analogue assumes the area driven by the wall pressure equals the open area. However, the area covered by the liner panel, S, is usually considered as reference rather than the open area, S_0 (comp. Figure 1(c)). The ratio σ of open and treated area is introduced as $\sigma = S_0/S$. This leads to a modified resonance frequency for liner panels, which depends on the total area of the panel instead of the neck area $\omega_0 = c\,\sqrt{\sigma S/VL}$.

2.1.2. The $\lambda/4$–resonator (Figure 1(d))

A very simple principle of an acoustic lining is the $\lambda/4$-resonator shown in Figure 1(d). It consists of a narrow tube, which is connected to the environment on one end and closed by a rigid wall on the other end. Due to the dimensions, the wave propagation in other directions than along the tube axis is negligible. The impedance function of such an undamped $\lambda/4$-resonator is described as $Z = -i\,\varrho_0\,c\,\cot(\omega\,l\,c^{-1}) = -i\,\varrho_0\,c\,\cot(He_l)$, where l denotes the depth of the tube from the open end to the rigid closure and He_l the related Helmholtz number.

2.1.3. The extended Helmholtz resonator model (EHR)

The extended Helmholtz resonator (EHR) model [1] finally combines elements of the mass-spring-damper analogue with the $\lambda/4$–resonator and adds possible damping inside the cavity. The EHR features a cotangent term as well as mass-like and dissipative terms. It describes the impedance of a damped Helmholtz resonator as

$$Z_{\mathrm{EHR}} = R_f + i\omega m_f - i\beta \cot\left(0.5\,\omega T_l - i\,0.5\,\varepsilon\right) = \frac{\left(R_f + i\omega m_f\right)\left(1 - e^{-\alpha}\right) + \beta\left(1 + e^{-\alpha}\right)}{1 - e^{-\alpha}}, \text{ with } \alpha = i\omega T_l + \varepsilon. \quad (2)$$

2.1.4. Other impedance models

The above models cover a variety of acoustic linings for aeroengines. The mass-spring-damper analogy was used by Tam and Auriault [2] to formulate a time domain impedance boundary condition. The extended Helmholtz resonator model, which was implemented by Chevaugeon et al. [3] and Richter et al. [4] to their discontinuous Galerkin and finite difference based CAA codes respectively, can approximate the $\lambda/4$–resonator as well as other typical models for aircraft liners (e. g. [5]). A more general approach would be obtained by describing the frequency response of the liner by a digital filter as found for instance in Özyörük and Long [6], Fung et al. [7], Fung and Ju [8], Reymen et al. [9]. However, using a digital filter at the same time means loosing the physical interpretation of the model parameters, which will be developed below. This interpretation allows to establish a straightforward connection between the liner structure and the resulting impedance.

2.2. Grazing flow model

For the modelling of the flow effect on the impedance under grazing flow conditions, two approaches will be presented in this section. Both have a potential range of application. The Ingard/Myers boundary condition is more qualified for low grid resolutions, whereas the resolved shear layer provides a stable and accurate alternative for higher grid resolutions [10]. The Ingard/Myers boundary condition [11] allows to describe the acoustic propagation with a plug flow assumption. Nevertheless, it shows an instability, especially for high grid resolutions. Besides the theoretically predictable effect of the flow on the impedance due to a modification of the incident angle [12] by the flow, a nonlinear flow effect exists. This effect can only be quantified by a measurement of the impedance under the grazing flow conditions as it is described in section 6.1.

2.2.1. The Ingard/Myers boundary condition

The impedance of a surface is originally defined as $Z = \hat{p}/\hat{v}_n$ without flow. Different from a hard wall, there is a high sensitivity of the sound field and attenuation towards the flow. The flow alters the angle of incidence on the lined surface for acoustic waves passing the boundary layer, which has an effect on the observed attenuation especially around the optimum. Additionally, the flow may alter the properties of the liner itself in a nonlinear manner. This is not addressed by the Ingard/Myers boundary condition. A general model for the linear flow effect on the impedance is given by Myers [11] assuming the continuity of the particle displacement over the infinite thin shear layer extending the previous work of Ingard [13]. The Ingard/Myers boundary condition [11] is given as $\hat{u}_n = \hat{p}\,Z^{-1} + \boldsymbol{u}_0 \cdot \boldsymbol{\nabla}\hat{p}\,(i\omega Z)^{-1} - \hat{p}\,(i\omega Z)^{-1}\boldsymbol{n}\cdot(\boldsymbol{n}\cdot\boldsymbol{\nabla}\boldsymbol{u}_0)$. The wall normal $\boldsymbol{n}$ is defined positive when pointing into the impedance surface. The additional terms describe the convection with the mean flow and the curvature of the impedance surface. The two additional terms become zero without a mean flow ($\boldsymbol{u}_0 = \boldsymbol{0}$). In this case the Ingard/Myers model returns to $Z = \hat{p}/\hat{v}_n$ and the assumed thin shear layer at the impedance surface vanishes.

2.2.2. Resolved boundary layers

The obvious method to include the flow effect on the impedance, is a resolved boundary layer with no slip condition at the impedance surface. This method has been applied for instance by Zheng and Zhuang [14] and Reymen et al. [9]. Both use artificial profiles for the boundary layer. Zheng and Zhuang [14] observe a convergence of the solution towards the solution using the Ingard/Myers boundary condition with a decreasing boundary layer thickness at the wall. Reymen et al. [9] do not provide such convergence studies. They use an artificially thickened boundary layer and cannot provide a correct prediction of the experiment. Realistic boundary layers from a CFD simulation are considered by Burak et al. [15]. They show that a correct prediction of the NASA grazing-flow-tube experiment can be obtained by a high-order CFD code. The resolved modelling of a grazing flow requires an adequate grid resolution

for both the acoustic scales and the boundary layer. When considering the thickness of the viscous sub layer as a minimum resolved length scale, the grid resolution would be dramatically increased from the acoustic limit. However, for viscous models in high resolution CAA simulations, the wall resolutions will meet this resolution limit.

2.3. Time domain impedance model derived from the extended Helmholtz resonator

Applying an inverse Fourier transform and combining the extended Helmholtz resonator model with the Ingard/Myers boundary condition one obtains a boundary condition for $\dot{u}'_n$

$$\frac{\partial u'_n}{\partial t}(t) = \frac{1}{m_f}\left[\mu(t) - (R_f + \beta)\, u'_n(t)\right] \underbrace{- \frac{1}{m_f}\, e^{-\varepsilon}\left[\mu(t - T_l) - (R_f - \beta)\, u'_n(t - T_l)\right] + e^{-\varepsilon}\frac{\partial u'_n}{\partial t}(t - T_l)}_{\text{storage term}}, \tag{3a}$$

where $\mu(t)$ arises from the Ingard/Myers boundary condition as

$$\mu(t) = p' + s_p, \quad \text{with} \quad \frac{\partial s_p}{\partial t} = \boldsymbol{u}_0 \cdot \boldsymbol{\nabla} p' - \boldsymbol{n} \cdot (\boldsymbol{n} \cdot \boldsymbol{\nabla} \boldsymbol{u}_0)\, p'. \tag{3b}$$

Equations (3a) and (3b) represent the implementation form of the EHR.

m_f is non-zero to allow the coupling of the time-domain impedance boundary condition through this parameter. Furthermore, it is found, that m_f defines another CFL limit. The maximum time step size for a stable solution is obtained to $\Delta t < m_f/c$. The EHR requires one variable to store all terms to be taken at previous times $t - T_l$. This is implemented using a circular buffer. With the simulation marching on in time, the full time series of this storage variable back to $t - T_l$ is required. The storage term is calculated and saved for each full step of the LDDRK only. The old time level for subsequent steps of the LDDRK is obtained from this storage variable at time levels close to $t - T_l$, by a filtering interpolation [16]. Old time levels up to ten time steps before $t - T_l$ are stored to have an adequate number of time samples for the interpolation. Furthermore, the time derivative $\dot{u}'_n(t - T_l)$ is not directly provided by the Runge-Kutta time marching scheme in 2N-storage form. To obtain a high-order finite difference approximation, seven time steps of u_n before the current one are stored in an own circular buffer. The time derivative for the storage term is then calculated by applying the seven-point central differencing scheme to this data.

Additional dissipation is identified as a possible treatment of the instability of the Ingard/Myers boundary condition. The terms of the auxiliary storage variable, which are evaluated at the time level $t - T_l$ in Eq. (3a) are summed up before they are spatially filtered. The convective and curvature terms of $\mu(t)$ are filtered after the time integration has been performed with the LDDRK. A second-order filter is applied.

3. Eduction of the model parameters from measurements

This section addresses the nonlinear effect of the grazing flow on the impedance. For this purpose, a measurement with a liner panel under grazing flow conditions is performed.

3.1. General outline of the eduction process

An optimisation procedure with the CAA-method is applied to calculate the impedance from the measurements in a flow impedance tube. The optimisation uses a control loop, which controls the deviation from the derived data from the experiment via an objective function. For both, simulation and experiment, discrete pressure data from the

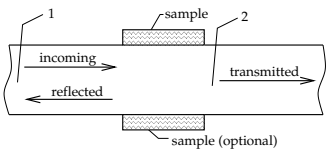

Figure 2: Sketch of the set-up for the calculation of the transmission and reflection coefficient

microphone positions is used to calculate reflection and transmission coefficients. The experimental data is based on a wave decomposition, which combines a downstream and upstream excitation of the liner sample in order to keep the resulting energy transmission, reflection and dissipation coefficients independent from reflections by the imperfect anechoic terminations. The energy transmission and reflection is then calculated based on the definition of these coefficients with flow according to Blokhintsev [17]

$$T = \left(\frac{\hat{p}_{\text{trans}}}{\hat{p}_{\text{base}}}\right)^2 \qquad \text{and} \qquad R = \frac{(1 - Ma_1)^2}{(1 + Ma_1)^2}\left(\frac{\hat{p}_{\text{refl}}}{\hat{p}_{\text{base}}}\right)^2, \tag{4}$$

where section 1 is considered to be the section with the incoming wave from the excitation and 2 is the section following the sample in the direction of sound propagation. The baseline amplitudes are denoted by the subscript base. The Mach number Ma is considered to be signed positive when the incoming acoustic waves propagate with the flow. The reflected pressure amplitude is calculated as $\hat{p}_{\text{refl}} = (\hat{p} - \hat{p}_{\text{base}})$. The transmitted pressure is the pressure in the section 2, based on a mode analysis in the experiment and assuming perfect anechoic boundary conditions for the numerical simulation, respectively.

The objective function is defined by the L_2-norm of the deviation between numerical and experimental reflection and transmission coefficients over all frequencies $E = \sum \left[\left(T_{\text{CAA}} - T_{\text{exp.}}\right)^2 + \left(R_{\text{CAA}} - R_{\text{exp.}}\right)^2\right]$. The five parameters of the EHR define the impedance of the sample. These parameters are varied in order to minimize the deviation of the energy coefficients from the experiment. The EHR model requires all parameters to be real and positive [1]. The according constraints are set in the optimisation. Further constraints account for m_f to be non-zero and not to small for the fixed CFL-number of the simulation. To avoid aliasing effects with discrete frequency data, the time lag T_l has been limited as well. The constrained nonlinear MATLAB optimisation procedure *fmincon* is used as optimization algorithm.

3.2. Identification of geometry parameters for the impedance models

A low frequency approximation of the cotangent term is obtained by a Laurent series expansion. For instance, the cotangent term of the $\lambda/4$–resonator can be replaced by a truncated Laurent series about $He_l = 0$ which results in the following approximation: $Z \approx -i\,\varrho_0\,c\left[He_l^{-1} - 1/3 He_l\right] = (i\omega)^{-1}\,\varrho_0\,c^2\,l^{-1} + i\omega\,\varrho_0\,l/3$. By considering terms of equal order in $i\omega$ as found for the mechanical analogue the mass- and spring-like contributions are identified for low frequencies. The corresponding low frequency limit of the EHR model is obtained in the same way by a Laurent series

Table 1: Low frequency limits of the impedance models.

	mass $(i\omega)$	**friction** (1)	**spring** $(\frac{1}{i\omega})$
Resonator panel	$\frac{\varrho_0 L}{\sigma}$	d	$\varrho_0\,c^2\,\frac{S}{V}$
$\lambda/4$**–resonator**	$\frac{1}{3}\varrho_0\,l$	-	$\varrho_0\,c^2\,\frac{1}{l}$
Ko [5]	$\frac{R_f}{\omega_f} + \frac{1}{3}\,\varrho_0\,l$	R_f	$\varrho_0\,c^2\,\frac{1}{l}$
Rienstra [1]	$m_f + \frac{1}{6}\beta\,T_l$	$R_f + \frac{2\beta\varepsilon}{T_l^2 + \left(\frac{\varepsilon}{\omega}\right)^2} + \frac{1}{6}\beta\,\varepsilon$	$\frac{2\beta\,T_l}{T_l^2 + \left(\frac{\varepsilon}{\omega}\right)^2}$

approximation to the linear order of α. In accordance with Rienstra [1], R_f and m_f are the resistance and reactance of the face sheet, respectively. The model abstracts the geometry to a time delay parameter $T_l/2$ in the cotangent, which can either be the time lag l/c of the $\lambda/4$-resonator or $V/(S\,c)$ of the mass-spring-damper analogue. A frequency dependent dissipative term, ε, is added to the cotangent. It corresponds to a damping inside the cavity fluid. β can be related to the open area ratio of the liner. The low frequency limits are summarised in Table 1.

4. Energetic analysis of the solution

The global conservation of the acoustic energy provides an instrument to measure the quality of a numerical solution as introduced by Eversman [18]. The approach is based on a balance of the acoustic energy flux entering the

duct from the source boundary and the outgoing fluxes over the lined wall and the terminal plane of the duct. In the absence of sound sources, the incoming acoustic power from the source boundary ($P = \int \boldsymbol{I} d\boldsymbol{S}$) should be equal to the sum of all outgoing power fluxes in time average. The definition of Morfey [19] is used for the acoustic energy and intensity. With liner, a global balance of the incoming and outgoing acoustic energy has to consider the flux over the liner as well.

5. Test case setup

5.1. Liner panel and impedance eduction

In the current paper, the liner panel shown in Figure 4 is used for all investigations. In a first step, the corresponding model parameters for this liner are obtained from a measurement with a liner sample in a flow impedance tube. The flow duct set up features a 80 mm × 80 mm test section of 220 mm length, in which a liner can be mounted to replace the lower wall. The plane liner samples fits into the test section and is sealed. Flush mounted microphones are positioned at the centreline of the upper wall in the up- and downstream duct sections. The numerical set-up for the impedance eduction according to section 3 uses a mesh of 1375 points with a mesh spacing of 8 mm. The CFL number is 0.15 to allow relatively small m_f. The non-reflective boundary conditions are implemented via the radiation/outflow boundary condition [20, 21]. 35 000 time steps are calculated in total to obtain a non-transient time series of 0.1 s which takes 3 minutes in real time on one core of a dual core AMD Opteron 244 processor.

5.2. Rearward sound radiation from the lined bypass duct of an aeroengine

(a) Mach number contours (b) Velocity distribution

Figure 3: Base flow field obtained by a preceding RANS simulation and liner

The second test case uses the model parameters obtained from the impedance eduction to simulate the effect of the liner considered in the experiment above on the sound radiation from the bypass duct of a long cowl nozzle in the presence of flow. The corresponding base flow profiles were obtained by a RANS simulation [22]. The Mach number distributions are shown in Figure 3. Two cases are considered, a two dimensional simulation under the assumption of a modal axisymmetric sound field and a three dimensional simulation. The relatively fine mesh, which is able to resolve the wall boundary layers and shear layers almost all over the computational domain, for this 2D simulation consists of 1.8×10^6 grid points. The simulation is carried out on two cores of an AMD Opreron 244 processor with 1.8 GHz. This takes 71 hours for 20000 time steps and 0.018 s in real time respectively. The three dimensional simulation uses a coarser mesh with only 7×10^6 grid points. This simulation takes 35 hours on 16 cores of the AMD Opteron 270 with 2 GHz for 10500 iterations and 0.02 s in real time respectively.

6. Results and discussion

6.1. Impedance Eduction

The resulting impedance functions are shown in Figure 4 for the downstream sound propagation. The EHR model parameters are given in Table 2. The impedance of the liner remains constant while the flow velocity is varied, which makes the extrapolation to $Ma = 0.9$ for the next test case more reasonable. The convergence of the impedance eduction is verified by the comparison of the resulting energy transmission, reflection and dissipation coefficients.

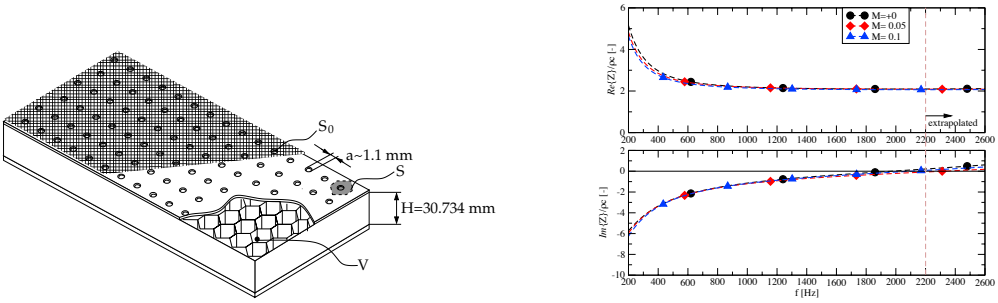

(a) Schematic of the investigated liner panel

(b) Frequency response of the educed impedance

Figure 4: Liner panel and its impedance

Table 2: EHR model parameters with plug flow profile, geometry based on an assumed open area ratio of $\sigma = 0.1$.

Ma [-]	$1/T_l$ [s^{-1}]	R_f [-]	$1/m_f$ [-]	β [-]	ε [-]	L [mm]	H [mm]
0.0	4570	2.04	965	0.990	0.134	1.33	37.6
0.05	4790	2.03	847	0.955	0.122	1.25	37.2
0.1	4740	2.06	892	0.977	0.071	1.28	36.7

6.2. *Interpretation of the resulting model parameters*

The result of the impedance eduction is further investigated by the corresponding liner geometry. The sample has a cavity depth of $H = 30.734$ mm. The open area cannot be determined due to the gauze covering. The educed geometrical parameters are given in Table 2 as well. Similar to the EHR model parameters, the geometrical parameters show only small variations with the Mach number for waves propagating downstream along the liner. There is a good agreement of the geometry parameters between the cases and a slight over prediction of the real geometry ($H = 30.73$ mm).

6.3. *Application of the model parameters in a realistic set up*

A two dimensional and a three dimensional simulation with liner are considered in this section. For comparison a fully hard walled nozzle is also simulated in 2D. All cases are based on an axisymmetric nozzle with axisymmetric base flow. The liner is placed inside the inner wall of the exit nozzle of the bypass duct as shown in Figure 6.3 as dark (red) wall texture. The base flow is obtained from a RANS simulation. It has been interpolated to the CAA mesh by a first order interpolation. The flow velocities at the walls are set to zero after the interpolation. In consequence, the wall velocity of the base flow is always zero. Thus, the Ingard/Myers boundary condition is not used. Furthermore, the base flow is filtered by a second order filter multiple times after the interpolation in case of the 2D simulation. This is found necessary to control the growth of unstable vortex structures inside the shear layers of the coaxial jet.

An overview of the resulting instantaneous three dimensional sound field is given in Figure 6.3. The simulations use a liner ranging from $x = -1.041$ to the end of the outer nozzle. The excitation frequency for the single $(m, n) = (8, 0)$ mode is 2.2 kHz. The corresponding directivity characteristics in the near field at $r = 1.5$ are compared in Figure 5. The two and the three dimensional simulations lead to similar results. However, the sound pressure level of the radiated field is predicted slightly higher by the 2D simulation.

6.3.1. *Acoustic energy considerations*

Finally, an analysis of the acoustic energy according to section 4 is carried out. The result is visualized in Figure 6. A control volume is defined, which includes the bypass and core duct as well as the radiation areas. The flux over the hard walls is assumed to be zero. The flux over the right domain boundary is also assumed to be negligibly small,

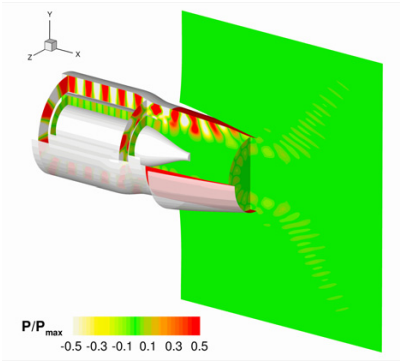

(a) Instantaneous pressure contours

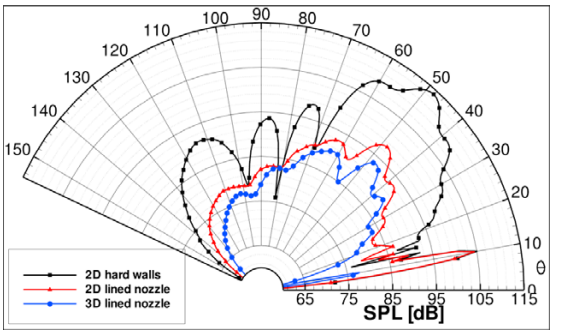

(b) Directivity

Figure 5: Instantaneous pressure contours and directivity

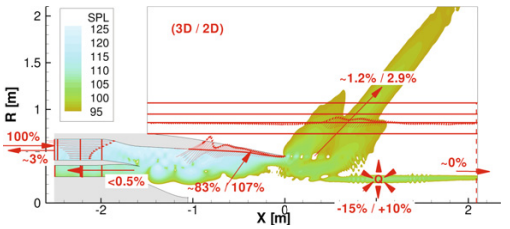

(a) Intensity analysis

Figure 6: Acoustic energy and intensity analysis

as the intensity cannot be calculated in the presence of vortices here. The flux of the acoustic energy in time average is integrated over the control surfaces shown in Figure 6 as thick lines. The conservation of the acoustic energy does not strictly apply in the given example, as the non-isentropic coaxial jet flow in the control volume violates the basic assumptions of this conservation according to Morfey [19]. However, under the assumption of a negligible source strength due to the shear layers, an approximate balance of the acoustic energy in the control volume should be realized. Thus, the incoming acoustic energy from the fan (left in the bypass duct, 100 %) should be equal to the sum of the outgoing energy fluxes over the liner, the back reflection into the bypass and core ducts and the radiated energy over the cylindrical shells around the nozzle. In case of the 3D simulation 15 % of the acoustic energy are annihilated inside the control volume. The grid resolution in the 3D simulation is close to the limit of 7 PPW. Thus, the result is probably affected by a higher dissipation than the over resolved 2D result. The 2D simulation shows a production of acoustic energy in the shear layers, which is not present in the 3D simulation. This production of acoustic energy leads to a global production, which manifests itself in a production of about 10 % of the input energy in the global balance. In the 3D case, the liner dissipates about 83 % of the acoustic energy originally input by the source. Due to the production of sound energy in the shear layers in the 2D case, the liner dissipates more energy than input by the source. 107 % of the input acoustic energy are dissipated over the liner in this case. Only a small fraction of the energy is reflected back into the bypass ($\approx$ 3 %) and core ($<$ 0.5 %) ducts for both of the cases. Altogether the lined ducts radiate about 2.9 % (2D) or 1.2 % (3D), whereas a hard walled nozzle would radiate 104 % of the acoustic energy according to the 2D simulation with a small production of acoustic energy inside the control volume included. Altogether, 2D and 3D simulations show similar radiation characteristics and levels with liner. Both simulations are affected by numerical errors; the 3D simulation shows significant dissipation especially inside the bypass duct, which

is revealed by comparing the 3 control planes in the bypass duct with each other. The 2D simulation on the other hand is affected by a production of acoustic energy inside the shear layers. However, the error is below 15 % of the overall energy. This corresponds to a maximum inconsistency of about 3.8 dB between the 2D and 3D result for the overall radiated acoustic energy.

7. Conclusions

The application of time domain impedance model in a aeroacoustic simulation has been demonstrated. It is starting from the eduction of the model parameters from measurements in an impedance flow tube, which provides energy transmission and reflection coefficients. The time domain impedance model used here is based on the extended Helmholtz resonator of Rienstra [1]. With the educed model parameters, this model provides an effective liner geometry by a relation of these parameters to a low frequency Helmholtz resonator model. Based on the educed model parameters, the liner is virtually implemented into the exit nozzle section of the bypass duct of an aeroengine under take-off conditions. The result is a simulated noise radiation and noise reduction pattern. Two and three dimensional simulations using the educed model parameters are carried out to provide a prediction of the attenuation of a higher azimuthal mode. The stable operation of the numerical method at this high flow speed with resolved boundary layers and with two coaxial shear layers and thermal boundary layers demonstrates the robustness of the present CAA-method. The liner largely reduces the sound radiation. Different from the fully hard walled case, where almost the full input energy is radiated to the far field, only a small fraction of the energy introduced at the main fan is radiated from the lined nozzle. The acoustic intensity analysis shows that the majority of the acoustic energy is dissipated in the liner panel. The result provides a prove of the numerical concept and general method. Practical aspects as the available space for the liner or its durability under the influence of hot burned gases in the mixing duct have not jet been considered. It is also important to note that the liner is originally designed as an inlet liner. It is not optimized for the specific application in the bypass. Such an optimization would be another application of a time domain impedance model. However, the computational time for two and three dimensional simulations are far too high for an optimisation with the real geometry in the design process.

8. Outlook: CAA on a Graphics Processing Unit

(a) GPU simulation, 2D

(b) CPU simulation, 3D

Figure 7: Instantaneous pressure contours obtained using isentropic models

To reduce the computational time and allow an optimization for the real geometry at lest with a modal axisymmetric approach, the CAA solver has been implemented to run on a graphic processing unit (GPU). The current simulation using the two dimensional mesh with 1.8×10^6 points takes about 40 minutes on a single NVIDIA Geforce 8800 GTX graphics card for 2×10^4 iterations. The code has been newly developed with respect to the specifics of a graphics processor. The development is platform independent. It is based on *C for graphics (CG)* by NVIDIA and proprietary in house libraries implementing the interface to the graphics processor. The libraries as well as the compiler work with any modern graphics processor with pixel shader units under Linux and Windows. Tested have been graphics

boards with GPU's of AMD-ATI and NVIDIA, both showing a similar speed up. The resulting pressure contours are shown in Figure 7. The GPU-CAA code has not yet reached the level of versatility, which is documented by the CPU based solver. Currently, it is limited to 2D and modal axisymmetric simulations, where an isentropic pressure density relation is assumed for the acoustic perturbation. However, the pressure contours are very similar between the GPU and CPU simulations using an isentropic assumption in 2D and 3D respectively. Altogether, the encouraging results demonstrate, that a complex application as a CAA simulation can be implemented platform independent on a modern graphics processor. The reduction of computational time achieved by this is in the order of 100 for the current example of the rearward sound radiation from a lined aeroengine bypass duct.

Acknowledgement

The authors acknowledge Piergiorgio Ferrante and Paul Murray at Alenia Aermacchi for providing the excellent liner sample and the helpful discussions. The authors acknowledge Christian Westphal for the visualisations. The funding was partly provided by the DFG project LIMIT.

[1] S. W. Rienstra, Impedance Models in Time Domain, Including the Extended Helmholtz Resonator Model, AIAA Paper 2006–2686, 2006.
[2] C. K. W. Tam, L. Auriault, Time-Domain Impedance Boundary Conditions for Computational Aeroacoustics, AIAA Journal 34 (5) (1996) 917–923.
[3] N. Chevaugeon, J.-F. Remacle, X. Gallez, Discontinous Galerkin Implementation Of The Extended Helmholtz Resonator Model In Time Domain, AIAA Paper 2006–2569, 2006.
[4] C. Richter, F. Thiele, X. D. Li, M. Zhuang, Comparison of Time–Domain Impedance Boundary Conditions by Lined Duct Flows, AIAA Paper 2006–2527, 2006.
[5] S.-H. Ko, Sound attenuation in lined rectangular ducts and its application to the reduction of aircraft engine noise, Journal of the Acoustical Society of America 50 (6, Part 1) (1971) 1418–1432, doi:\bibinfo{doi}{10.1121/1.1912784}.
[6] Y. Özyörük, L. N. Long, A time-domain implementation of surface acoustic impedance condition with and without flow, AIAA Paper 1996–1663, 1996.
[7] K.-Y. Fung, H. B. Ju, B. Tallapragada, Impedance and its time-domain extensions, AIAA Journal 38 (1) (2000) 30–38.
[8] K.-Y. Fung, H. B. Ju, Broadband time-domain impedance models, AIAA Journal 39 (8) (2001) 1449–1454.
[9] Y. Reymen, M. Baelmans, W. Desmet, Time-Domain Impedance Formulation suited for Broadband Simulations, AIAA Paper 2007–3519, 2007.
[10] C. Richter, F. Thiele, The Stability of Time Explicit Impedance Models, AIAA Paper 2007–3538, 2007.
[11] M. K. Myers, On the acoustic boundary condition in the presence of flow, Journal of Sound and Vibration 71 (8) (1980) 429–434.
[12] X. D. Li, C. Richter, F. Thiele, Time-Domain Impedance Boundary Conditions for Subsonic Mean Flow, Journal of the Acoustical Society of America 119 (5) (2006) 2665–2676.
[13] U. Ingard, Influence of fluid motion past a plane boundary on sound reflection, absorption, and transmission, Journal of the Acoustical Society of America 31 (7) (1959) 1035–1036.
[14] S. Zheng, M. Zhuang, Verification and Validation of Time-Domain Impedance Boundary Condition in Lined Ducts, AIAA Journal 43 (2005) 306–313.
[15] M. O. Burak, M. Billson, L.-E. Eriksson, S. Baralon, Validation of a Time & Frequency Domain Grazing Flow Acoustic Liner Model, AIAA Journal 47 (8) (2008) 1841–1848.
[16] C. Richter, Liner impedance modeling in the time domain with flow, Ph.D. thesis, Technische Universität Berlin, URL http://opus.kobv.de/tuberlin/volltexte/2010/2403/, 2009.
[17] D. I. Blokhintsev, Acoustics of a nonhomogeneous moving medium, National Advisory Committee for Aeronautics, Washington, 1956.
[18] W. Eversman, Acoustic Power in Lined Ducts, AIAA Paper 2004–2904, 2004.
[19] C. L. Morfey, Acoustic Energy in Non-Uniform Flows, Journal of Sound and Vibration 14 (2) (1971) 159–170.
[20] C. K. W. Tam, C. Webb, Dispersion-Relation-Preserving Finite Difference Schemes for Computational Aeroacoustics, Journal of Computational Physics 107 (2) (1993) 262–281.
[21] C. Bogey, C. Bailly, Three-dimensional non-reflective boundary conditions for acoustic simulations: Far field formulation and validation test cases, Acta Acustica united with Acoustica 88 (2002) 462–471.
[22] J. Yan, L. Panek, F. Thiele, Simulation of jet noise from a long-cowl nozzle with serrations, AIAA Paper 2007-3625, 2007.